ACS APPLIED MATERIALS & INTERFACES

www.acsami.org

Research Article

Hard- and Soft-Coded Strain Stiffening in Metamaterials via Out-of-Plane Buckling Using Highly Entangled Active Hydrogel Elements

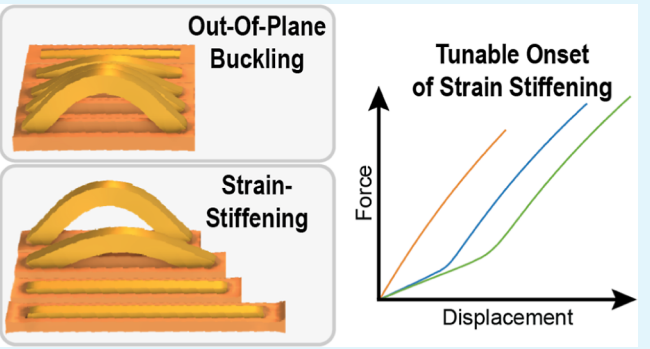
Oliver Skarsetz, Robin Mathes, Ricarda Sophia Schmidt, Moritz Simon, Viacheslav Slesarenko,* and Andreas Walther*

Cite This: *ACS Appl. Mater. Interfaces* 2024, 16, 38511−38519

Read Online

ACCESS | Metrics & More | Article Recommendations | Supporting Information

ABSTRACT: Metamaterials show elaborate mechanical behavior such as strain stiffening, which stems from their unit cell design. However, the stiffening response is typically programmed in the design step and cannot be adapted postmanufacturing. Here, we show hydrogel metamaterials with highly programmable strain-stiffening responses by exploiting the out-of-plane buckling of integrated pH-switchable hydrogel actuators. The stiffening upon reaching a certain extension stems from the initially buckled active hydrogel beams. At low strain, the beams do not contribute to the mechanical response under tension until they straighten with a resulting step-function increase in stiffness. In the hydrogel actuator design, the acrylic acid concentration hard-codes the configuration of the metamaterial and range of possible stiffening onsets, while the pH soft-codes the exact stiffening onset point after fabrication. The utilization of out-of-plane buckling to realize subsequent stiffening without the need to deform the passive structure extends the application of hydrogel actuators in mechanical metamaterials. Our concept of out-of-plane buckled active elements that stiffen only under tension enables strain-stiffening metamaterials with high programmability before and after fabrication.



KEYWORDS: *strain stiffening, out-of-plane buckling, highly entangled hydrogels, actuators, programmable metamaterials*

Downloaded via UNIV FREIBURG on December 20, 2024 at 23:37:10 (UTC).
See https://pubs.acs.org/sharingguidelines for options on how to legitimately share published articles.

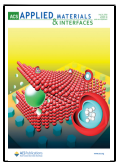
1. INTRODUCTION

Biological tissues greatly stiffen under high external stress to protect themselves from structural damage.[1] Many polymer networks possess a similar stiffening behavior, where polymer chain coils initially uncoil under applied strain until reaching a critical value. Thereafter, the initial compliant chain bending transitions into chain stretching with a resulting stiffening.[2,3] Generally, the network structure predefines the resulting J-shaped stress−strain curves.[4−9] Strain stiffening is an important biological mechanism for self protection and gives inspiration for synthetic materials to improve reliability and durability, and avoid material failure.

Mechanical metamaterials are artificial materials with unconventional mechanical behavior originating from their internal architecture.[10,11] Macroscopic responses to applied forces such as negative Poisson's ratio,[12−14] shape matching,[15] and shape morphing[16] can be programmed by unit cell design. Approaches for strain-stiffening metamaterials have focused on harnessing self contact between metamaterial elements under compression[17] or the integration of structural elements that show a transition from bending- to stretching-dominated under tension.[18] In these examples, the mechanical response is "hard-coded" during metamaterial manufacturing. The initial design defines the mechanical behavior without possibilities for an on-demand change of shape and behavior after fabrication. To overcome this limitation, metamaterials with active elements allow "soft-coding", that is, reprogramming of the architecture and behavior after fabrication. The introduction of different materials such as thermally programmable liquid crystal polymers,[19−22] shape memory polymers,[23] stress-relaxing polylactic acid filaments,[24] and magnetic materials[25−28] into metamaterials has given rise to architectures capable of altering their shape after fabrication.

Stimulus-responsive hydrogels represent an interesting candidate for engineering the active components in metamaterial architectures due to their high programmability with multiple stimulus responses. The active hydrogels act as muscles triggering the deformation of the passive frame by pushing, pulling,[29] or bending.[30−32] Simple swelling of hydrogel metamaterials can influence the stress−strain behavior due to global swelling or shrinkage of the entire

Received: April 26, 2024
Revised: June 10, 2024
Accepted: June 24, 2024
Published: July 9, 2024



© 2024 The Authors. Published by American Chemical Society

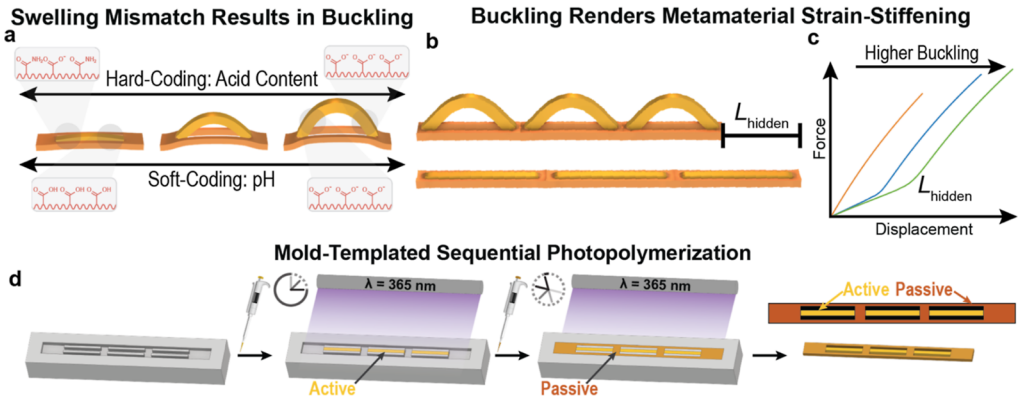


Figure 1. Schematic illustration of the hard- and soft-coded out-of-plane buckling of active struts in hydrogel metamaterials with resulting tunable strain stiffening and the mold-templated sequential photopolymerization fabrication technique. (a) The active beams swell more than the passive frame and buckle out of plane. Varying the acid amount hard-codes while the pH soft-codes the swelling of the active beam. (b) The out-of-plane buckling of the active beams gives rise to strain-stiffening metamaterials, where the buckled active beams decrease their curvature with increasing deformation. Upon reaching the onset of stiffening, the active beams fully straighten and contribute to the stiffness. (c) The hard- and soft-coded buckling degrees define the onset of stiffening in the resulting force−displacement curves. (d) Metamaterial fabrication method of sequential photopolymerization using PTFE molds.

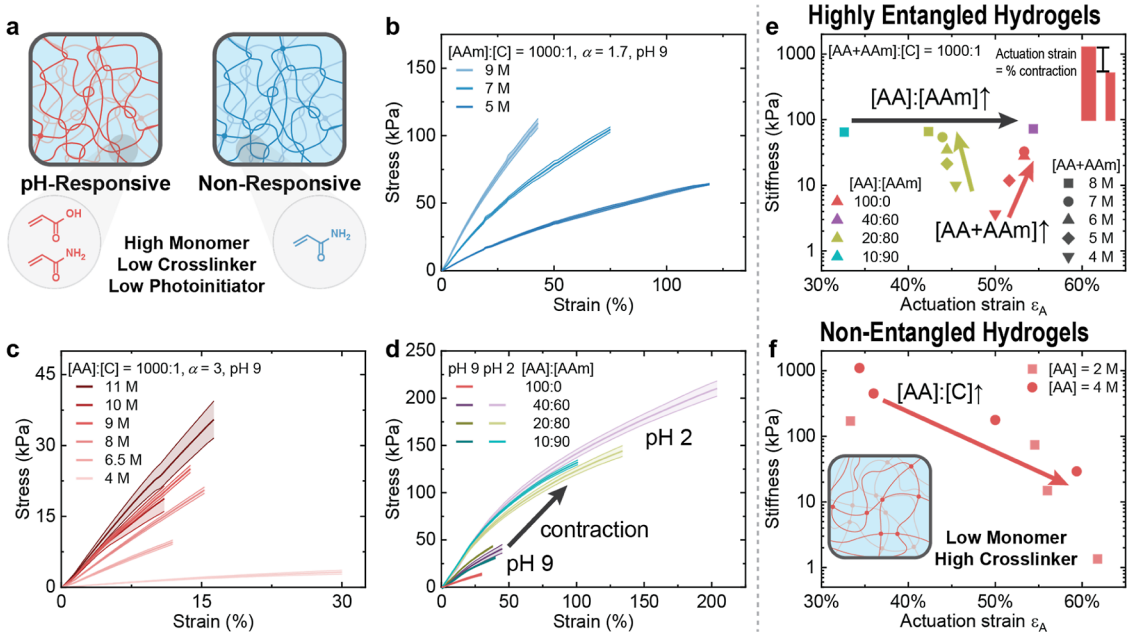


Figure 2. Mechanical testing and actuation performance of the developed pH-responsive p(AA-*co*-AAm) and nonresponsive $pAAm_{100}$ highly entangled hydrogels. (a) The developed dual material hydrogel system consists of nonresponsive $pAAm_{100}$ and responsive p(AA-*co*-AAm) hydrogels. Polymerization at high monomer and low cross-linker concentration results in high concentration of entanglements that further stiffen the hydrogels. (b) Tensile test of nonresponsive $pAAm_{100}$ with varying [AAm] = 9 M − 5 M and [AAm]:[C] = 1000:1 after equilibration to α = 1.7 in 50 mM $NaHCO_3$ buffer at pH 9. (c) Tensile tests of pH-responsive pAA_{100} with varying [AA] = 4 M − 11 M at [AA]:[C] = 1000:1 after equilibration to α = 3 in 50 mM $NaHCO_3$ buffer at pH 9. (d) Tensile tests of pH-responsive p(AA-*co*-AAm) hydrogels with varying [AA]:[AAm] ratios at [AA + AAm] = 8 M and [AA]:[C] = 1000 after equilibration at pH 9 (50 mM $NaHCO_3$) and pH 2 (50 mM citric acid). (e) Overview of stiffness (obtained from indentation tests) versus actuation strain of varying p(AA-*co*-AAm) hydrogels with varying [AA]:[AAm] at [AA] = 4 M − 8 M. (f) For comparison, the stiffness versus actuation strain of varying pAA_{100} hydrogels with [AA] = 2 M − 4 M and [AA]:[C] = 25:1−300:1. The data in (e,f) was derived from indentation tests (Figure S1).

architecture.[33] However, swelling of hydrogel-based metamaterials is almost inevitably accompanied by a change in size, which does not allow their application when the total dimensions have to be kept constant. Furthermore, simple swelling and drying fall short of the advanced responsiveness that can be coded chemically into responsive hydrogels. Overall, stimulus-responsive hydrogels have rarely been incorporated into metamaterial architectures due to the soft and brittle nature of hydrogels. To improve mechanical robustness, double network[34−37] or highly entangled hydrogel network[38,39] approaches can be pursued. Furthermore, stimulus-responsive double network hydrogels have been developed[40−42] yet not been introduced into soft-coded metamaterials.

Here, we introduce a fully hydrogel-based metamaterial with hard- and soft-coded strain-stiffening responses by implementing pH-responsive active beams into a passive hydrogel frame. Due to the different response for pH-gated swelling, the active

https://doi.org/10.1021/acsami.4c06610
ACS Appl. Mater. Interfaces 2024, 16, 38511−38519

beams buckle out of plane while keeping the frame dimensions unchanged. Upon metamaterial stretching, the buckled beams initially do not contribute to the stiffness until the beams straighten, which results in stepwise stiffening. The acid content of the highly entangled hydrogel actuators hard-codes the swelling range before fabrication, while the pH soft-codes the swelling after fabrication. Since the swelling degree defines the onset of the strain stiffening, the force−displacement curves are hard- and soft-coded, as well.

2. RESULTS AND DISCUSSION

Our fully hydrogel-based strain-stiffening mechanical metamaterial consists of a rectangular, passive, non-pH-responsive, and noncharged hydrogel frame (orange) with incorporated active pH-responsive polyelectrolyte beams (yellow; colors reflect the images below, Figure 1). Upon immersion of the as-prepared metamaterials at high pH, the active beams buckle out of plane almost immediately due to the higher swelling compared with the frame. Varying the acid concentration in the polyelectrolyte parts hard-codes the possible swelling range, whereas adjustment of the pH soft-codes the swelling by changing the charge density (Figure 1a). The active beams do not contribute to the overall stiffness until they fully straighten and gradually return to the metamaterial plane upon metamaterial stretching (Figure 1b). The onset point, after which the force−displacement curve stiffens stepwise, depends on the swelling degree, allowing it to be hard-coded as well as soft-coded (Figure 1c).

For the fabrication of the multimaterial metamaterials, we desired a simple fabrication technique allowing for the fabrication of each hydrogel material with a single component and without tedious reinfiltration procedures as needed for double network gels.[34,36] To this end, we fabricated the hydrogel metamaterials via sequential photopolymerization using PTFE molds by first polymerizing the active beams, followed by polymerizing the passive frame in a second step (Figure 1d). The dual material hydrogel metamaterial consists of two hydrogels, where the active beams are pH-responsive, while the passive frame is nonresponsive. Before combining the two materials into the metamaterial, the respective active and passive hydrogels are optimized individually. To increase mechanical robustness and crack resistance of the composite hydrogel metamaterial, we used the concept of highly entangled hydrogels, in which entanglements outnumber covalent cross-links, allowing the realization of hydrogels with high strength, toughness, and fatigue resistance.[38,39] This can be achieved by a polymerization at high monomer concentration with a small amount of initiator and at a high ratio of monomer to cross-linker (Figure 2a). For the passive frame, we screened recipes for highly entangled polyacrylamide (pAAm) as recently reported {[AAm] = 5 M − 9 M, initiator-to-cross-linker ratio [I]:[C] = 0.4 (I = lithium phenyl-2,4,6,-trimethylbenzoylphosphinate (LAP) initiator; C = *N*,*N*′-methylenebisacrylamide)}.[38,39] To maximize the hydrogel stiffness, we opted for a cross-linking ratio of [AAm]:[C] = 1000:1. For the active beams, we developed completely new poly(acrylic acid) (pAA) hydrogel actuators based on the same concept ([AA] = 4 M − 11 M, [I]:[C] = 0.4:1, [AA]:[C] = 1000:1).

We first discuss the mechanical tensile properties of the hydrogels (prepared in molds with 20 × 4 × 2 mm^3) after swelling to equilibrium at pH 9 and pH 2. A more than 1000-fold volumetric excess of 50 mM $NaHCO_3$ and 50 mM citric acid buffers is used to ensure identical pH equilibration independent of the employed acid concentration. The swelling lengths at pH 9 and pH 2 allow calculation of the respective 1D swelling factors $\alpha = L/L_{prepared}$ and the pH-responsive actuation strain $\varepsilon_A = 1 - L_{pH2}/L_{pH9}$. ε_A quantifies how much % the hydrogel contracts from its fully swollen state during pH-triggered actuation. To understand the mechanical property space, we first synthesized $pAAm_{100}$ (subscript indicates 100 mol % AAm) hydrogels at different total concentrations during the synthesis, i.e., [AAm]. Equilibration of the as-prepared hydrogels at pH 9 leads to a swelling factor α = 1.7. Tensile tests reveal that the stiffness of the $pAAm_{100}$ hydrogels increases from 70 kPa to 318 kPa while the elongation at break ε_B decreases from 119% to 43% when increasing [AAm] from 5 M to 9 M (Figure 2b). Like $pAAm_{100}$, we synthesized different pH-responsive pAA_{100} hydrogels. At pH 9, pAA_{100} equilibrates to a much higher swelling factor of α = 3. Tensile tests of the swollen hydrogels show lower stiffnesses and lower ε_B < 30% (Figure 2c) compared to $pAAm_{100}$. The stiffness of pAA_{100} increases from 14 kPa to 200 kPa, while the ε_B decreases from 30% to 16% when increasing [AA] from 4 M to 11 M. To reduce the swelling and further tune the hydrogel properties, we partly substituted AA with AAm in hydrogels prepared at 8 M to obtain p(AA-*co*-AAm) copolymer hydrogels with [AA]:[AAm] varying from 10:90 to 40:60. At pH 9, the stiffnesses reach around 125 kPa with the ε_B below 40% (Figure 2d, lower curves). At pH 2, the different p(AA-*co*-AAm) hydrogels contract to swelling factors α between 1.3 and 1.5, which results in a doubling of the stiffness to 236 kPa and ε_B up to 210% (Figure 2d, upper curves).

Furthermore, we calculated the pH-responsive actuation strain $\varepsilon_A = 1 - L_{pH2}/L_{pH9}$ for different p(AA-*co*-AAm) hydrogel compositions and conducted additional indentation tests (Figure S1) to allow fair comparison between the highly entangled hydrogels (Figure 2e) and brittle nonentangled gels synthesized for comparison (Figure 2f). A comparison of the stiffnesses in the swollen state with the pH-dependent actuation strains ε_A allows for a comprehensive visualization of the available property space (Figures 2e and S2). The stiffness of pAA_{100} increases from 4 kPa to 33 kPa when increasing the [AA] concentration during the synthesis from 4 M to 7 M, while the actuation strain ε_A remains constant around 52% (red symbols in Figure 2e). The p(AA-*co*-AAm) copolymer hydrogels with [AA]:[AAm] varying from 10:90 to 40:60 synthesized at a constant monomer concentration (squares in Figure 2e) show a near constant stiffness of 70 kPa, but a reduction of the fraction of AA leads to a consistent reduction in actuation strain ε_A from 54% to 32%. Like the pAA_{100} hydrogel, when increasing the monomer concentration during synthesis from 4 M to 7 M at constant AA content, e.g., $p(AA_{20}$-*co*-$AAm_{80})$, the stiffness increases from 10 kPa to 54 kPa, whereas the actuation strain ε_A remains constant around 43% (green symbols in Figure 2e). This means that the stiffness can be engineered to different levels without affecting the pH-responsive actuation behavior. This is useful in applications where struts of different stiffness but same actuation are required.

As a critical comparison, Figure 2f depicts data obtained for the stiffness versus pH-responsive actuation strain in classical, nonentangled hydrogels. In such tightly chemically cross-linked hydrogels that recruit stiffness from chemical cross-links and not from entanglements, pAA_{100} stiffness increases by increasing the cross-linker concentration at low monomer

https://doi.org/10.1021/acsami.4c06610
ACS Appl. Mater. Interfaces 2024, 16, 38511−38519

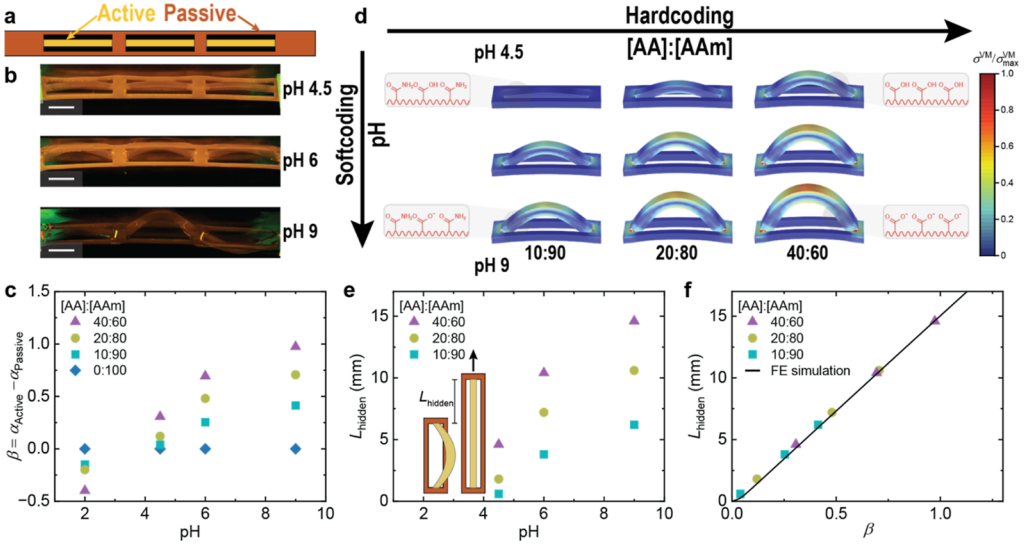


Figure 3. Soft- and hard-coding the out-of-plane buckling of the active beams via variation of [AA]:[AAm] and pH. (a) The strain-stiffening hydrogel metamaterial consists of three rectangular unit cells with 15 mm active beams. (b) Fabricated metamaterial with p(AA_{20}-*co*-AAm_{80}) (8 M; [AA + AAm]:[C] = 1000:1) active beams and $pAAm_{100}$ frame (5 M; [AAm]:[C] = 1000:1) at different pH. Scale bar 10 mm. (c) Experimental data: $\beta = \alpha_{active} - \alpha_{passive}$ quantifies the difference in swelling. At higher pH and higher [AA]:[AAm], the pAA_{100} hydrogels have a higher swelling factor α_{active}, while $\alpha_{passive}$ is constant at 1.7. (d) Finite element (FE) simulation predicts the out-of-plane buckling from the swelling mismatch with experimentally obtained α values. Changing the [AA]:[AAm] ratio from 40:60 to 10:90 hard-codes the extent of active beam swelling. Furthermore, the equilibration at pH 4.5 to pH 9 soft-codes the buckling extent. Von Mises stress σ_{max}^{VM} = 35 kPa. (e) Experimental data: The hidden length L_{hidden} depends on β as $L_{hidden} = L_0 \times \beta$. At higher pH and higher [AA]:[AAm], L_{hidden} is greater due to the greater length of the buckled active beam. (f) The L_{hidden} linearly depends on the β, independent of hard or soft coding. FE simulation verifies the relationship.

concentrations. At high [AA]:[C] = 25:1 and [AA] = 4 M, the stiffness reaches up to E = 1097 kPa with a low pH-responsive actuation strain ε_A of 33% (Figure 2f). However, the obtained hydrogel breaks into pieces during swelling due to its brittleness. At a lower [AA]:[C] = 300:1, the stiffness decreases 2 orders of magnitude and reaches 29 kPa and the pH-responsive actuation strain ε_A increases to 62%. The same coupling of stiffness and actuation appears for the pAA_{100} hydrogels at [AA] = 2 M, which reach similar actuation strain ε_A values but lower stiffnesses.

From these data, it becomes clear that the actuation strain and stiffness are strongly inversely correlated parameters in classical gels and cannot be designed independently. In contrast, for the highly entangled gels, the pH-responsive actuation strain can be kept relatively constant, while the stiffness can be increased by simply increasing the monomer concentration. Additionally, the highly entangled gels reached higher stiffness values without embrittlement.

Overall, highly entangled single network hydrogels prepared from high monomer and low cross-linker concentration serve as an ideal platform to overcome the stiffness−actuation trade-off and allow independent variation of actuation strain and stiffness of responsive p(AA-*co*-AAm) hydrogel networks. This beneficial material property is of general relevance to responsive hydrogel materials. For further metamaterial studies, we selected the 5 M $pAAm_{100}$ as frame material due to the highest elongation at break and low stiffness and 8 M p(AA-*co*-AAm) as active beam material due to higher stiffness and elongation at break as compared to pAA_{100}. Varying [AA]:[AAm] from 10:90 to 40:60 allows hard coding of the active beam swelling.

As a demonstration of how the developed p(AA-*co*-AAm) gel system integrates into strain-stiffening hydrogel metamaterials, we designed a metamaterial geometry with the tunable out-of-plane buckling of active beams. The strain-stiffening hydrogel metamaterial consists of three rectangular unit cells of passive $pAAm_{100}$ frame and active p(AA-*co*-AAm) beams connected in series (Figure 3a). Varying the AA comonomer ratio hard-codes the active beam length at a specific pH as a function of the AA content, whereas the pH soft-codes this length for each of them. The active beam expands more than the surrounding frame due to its higher swelling factor, which results in an immediate out-of-plane buckling.

As an example, we show the metamaterial soft coding at varying pH values (Figure 3b). With increasing pH, the buckled beam length increases. Note that the buckling direction is defined by minuscule imperfections during fabrication. However, the buckling direction does not affect the hard-coding, soft-coding, or strain-stiffening behavior. Qualitatively, the length of the buckled beam increases with a higher pH or [AA]:[AAm] ratio (Movie S1). The swelling mismatch can be quantitatively described with the swelling difference $\beta = \alpha_{active} - \alpha_{passive}$, where $\alpha_{passive}$ is identical for all pH levels (Figure 3c). Increasing the [AA]:[AAm] ratio from 10:90 to 40:60 tunes the swelling difference β from 0.4 to 1.0 at pH 9. The equilibration at decreasing pH decreases β. Below pH 4.5, β is negative, meaning that the active beams become smaller than the passive frame. This pulling on the frame is not useful for the proposed strain-stiffening approach and is not further pursued. The soft coding of the active beam length is reversible and can be repeated with consistent intensity through repeated pH fluctuations (Figure S3). In addition to experiments, FE simulations predict and further verify the out-of-plane buckling of the active beams, where experimentally determined α and stiffness values serve as input (Figure 3d). pH = 4.5 and high [AA]:[AAm] = 40:60 results in a buckled beam length similar to that at pH 9 and low [AA]:[AAm] = 10:90.

https://doi.org/10.1021/acsami.4c06610
ACS Appl. Mater. Interfaces 2024, 16, 38511−38519

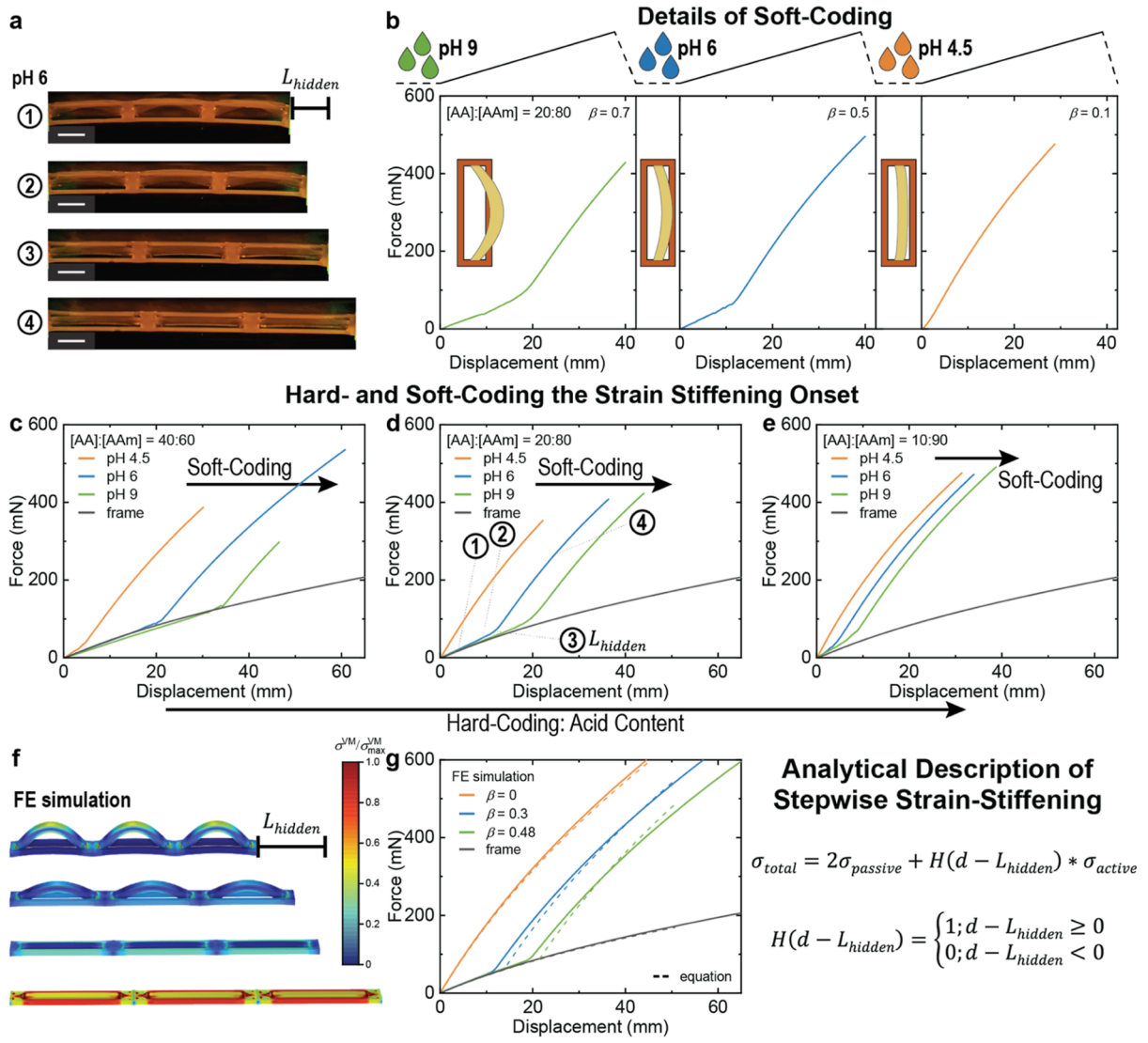


Figure 4. Tensile tests of different hard- and soft-coded strain-stiffening metamaterials with the respective FE simulation and analytical description. (a) Metamaterial from p(AA_{20}-*co*-AAm_{80}) (8 M; [AA + AAm]:[C] = 1000:1) active beams with $pAAm_{100}$ frame (5 M; [AAm]:[C] = 1000:1) under tensile deformation after equilibration at pH 6. The buckled active beams align under applied tensile deformation. At the onset of stiffening, the beams align and contribute to stiffness. Scale bar 10 mm. (b) Force−displacement curves of one metamaterial geometry after three times subsequently equilibrating and stretching to 40 mm displacement. (c) Hard-coding the [AA]:[AAm] ratio to 40:60 results in great variation in the soft-coded onset of stiffening. (d) Hard-coding the [AA]:[AAm] ratio to 20:80 decreases the onset of stiffening. (e) Hard-coding the [AA]:[AAm] ratio to 10:90 allows smaller soft-coded variation in the onset of stiffening. Numbers mark the different snapshots at the different displacements from Figure 3a. (f) FE simulation using the experimental α from Figure 2d validates the experiments. σ_{max}^{VM} = 35 kPa. (g) The resulting tensile curves are similar to the experimentally observed curves. The proposed theoretical definition of the stepwise strain stiffening is in agreement with the FE simulation.

The hidden length $L_{hidden} = L_{active} - L_{passive} = L_0 \times \beta$ describes the difference in length of the active and passive beam in the metamaterial geometry and directly correlates with the onset of stiffening. Changing the comonomer ratio or pH tunes L_{hidden} from 0 mm to 15 mm, as summarized in Figure 3e. A comparison of the L_{hidden} to the β reveals its linear dependence, irrespective of whether variation of pH or [AA]:[AAm] ratio tunes the swelling (Figure 3f). The corresponding FE simulations also capture this linear dependency.

After obtaining the means for programming by both hard- and soft-coding the swelling behavior of the hydrogels embedded into the passive frame, we experimentally assessed the strain-stiffening behavior of the resulting metamaterials under tensile deformation. Figure 4a exemplarily depicts the tensile test of the metamaterial with [AA]:[AAm] = 20:80 active beams with β = 0.5 after equilibration at pH 6. (1) Initially, the active beams buckle out-of-plane and possess a hidden length corresponding to the current pH level and acid comonomer ratio. (2) Under applied tensile deformation, the passive frame stretches and the active beams gradually align with the load direction without contributing to the stiffness. (3) Upon reaching the onset of stiffening, the active beams fully straighten and contribute to the stiffness. (4) Further deformation stretches both the passive frame and active beams together.

Figure 4b shows force−displacement curves for one metamaterial specimen stretched three times in a row after soft-coding under different pH. The metamaterial has an initial

https://doi.org/10.1021/acsami.4c06610
ACS Appl. Mater. Interfaces 2024, 16, 38511−38519

length of $L = L_0 \times \alpha_{passive}$ = 87 mm after equilibration (Figure S4). At pH 9, the central beam swells to β = 0.7 and buckles out of plane, which means that initially, only the passive frame contributes to the force response of the metamaterial. After 20 mm displacement, the active beam returns into the main plane, which results in a stiffness increase by a factor of 4. After unloading the specimen and equilibrating it at pH 6 (β = 0.5), the subsequent loading demonstrates strain stiffening with the onset shifted to 16 mm. Notably, the slopes of the force−displacement curves remain almost identical with the first loading. The third loading after equilibration at pH 4.5 (β = 0.1) shows a high initial stiffness with no further stiffening since the length of both passive and active beams is almost the same at this pH. Likewise, sequential equilibration of a metamaterial at repeating high and low pH results in identical force−displacement curves (Figure S5).

Furthermore, the acid amount hard-codes the range of possible onset values. Figure 4c−e gives an overview of the tensile tests of metamaterials with different hard-coded [AA]:[AAm] ratios. For the metamaterial with [AA]:[AAm] = 40:60 active struts, the maximal achievable onset of the strain stiffening is around 34 mm at pH 9 (Figure 4c). As seen for the lower [AA]:[AAm] ratios 20:80 (Figure 4d) and 10:90 (Figure 4e), the maximal value of the observed onset decreases with a decrease in [AA]:[AAm]. The tests on the stand-alone active hydrogels proved the independent tunability of actuation strain and Young's modulus (see Figure 2b). In this example, the slopes of the force−displacement curves are almost identical because the employed active hydrogel beams with different [AA]:[AAm] ratios possess similar stiffness values (see Figure 4c−e). The choice of hydrogel defines the system stiffnesses at the initial (before stiffening) and final (after stiffening) stages of tensile loading. Since the active beams do not contribute to the mechanical response at the beginning stages of loading of the metamaterial, the force−displacement curves stand in good agreement with the passive frame metamaterial without active beams. To summarize, the [AA]:[AAm] ratios define the range of achievable onsets, while pH soft-codes the exact onset value.

Numerical and analytical models also capture the swelling behavior of active beams and its effect on strain stiffening. For FE simulations, we selected the active metamaterial with [AA]:[AAm] = 20:80 and used the necessary swelling factor β versus pH dependencies as well as Young's moduli from experiments on stand-alone active hydrogels in Figure 2. The simulations consisted of two steps: swelling and stretching (Figure 4f). Figure 4g shows the resulting force−displacement curves obtained for different swelling factors β. The numerically obtained curves show good agreement with the experimental curves (Figure 4d,g). Like in experiments, the force−displacement curves before stiffening match the force−displacement curve obtained for the passive frame only, and the poststiffening regimes have almost identical slopes. A straightforward analytical model approximates the strain-stiffening behavior observed in the experiments and FE simulations. Since active and passive elements are placed in parallel in the unit cells, the resulting stress can be expressed as $\sigma_{total} = 2\sigma_{passive} + \sigma_{active} \times H[d - L_{hidden}(\beta)]$. $\sigma_{passive}$ and σ_{active} correspond to stresses in the passive and active beams and $H[d - L_{hidden}(\beta)]$ is a Heaviside function that takes a value of 1 when the applied displacement is larger than L_{hidden}, which depends on β. Assuming incompressible neo-Hookean models for both passive and active materials with shear moduli of $\mu_{passive}$ and μ_{active} correspondingly, the full expression for the resulting stress is $\sigma_{total} = 2\mu_{passive}[(1 + d/L) - (1 + d/L)^{-2}] + \mu_{active}\{L^{-1}[L + d - L_{hidden}(\beta)] - L^2[L + d - L_{hidden}(\beta)]^{-2}\} \times H[d - L_{hidden}(\beta)]$. The resulting dashed force−displacement curves in Figure 4g show good agreement with the curves obtained from FE simulations as well as with experimentally observed curves (Figure 4d). Despite minor differences between 3D numerical simulations and predictions of the analytical model, the latter gives a good first estimate for designing (hard-coding) metamaterials with tunable (soft-coding) strain stiffening.

3. CONCLUSIONS

We have introduced a straightforward design of all-hydrogel mechanical metamaterials with tunable strain stiffening utilizing the out-of-plane buckling of beams made of active hydrogels. The core concept relies on swollen, buckled beams not contributing to the overall stiffness of the metamaterial until the point when they fully return to the main plane of the metamaterial. Following the idea of programmable metamaterials, we distinguish the hard coding and soft coding of the resulting strain stiffening.

Furthermore, we showed that polymerizing networks with a high number of entanglements from high monomer and low cross-linker concentration serve as an ideal platform to obtain single network hydrogels with independent tunability of stiffness and actuation strain by variation of acid comonomer ratio or monomer concentration. Implemented into active beams, the swollen length depends on the hard-coded acid comonomer ratio and the soft-coded pH variation. The length of the active beams further defines the onset of strain stiffening as they remain mechanically hidden in the buckled state. After reaching the onset of stiffening, the beams aligned and contributed to the overall stiffness. Experimentally and numerically, we demonstrated the tunability of the stiffening onset and determined that the stiffness before and after the onset is almost identical for different comonomer ratios thanks to disentanglement of the Young's moduli and swelling state of the developed hydrogels. The presented concept of hidden active beams that are activated in tension-only mode is expandable to more complex metamaterials as well as tensegrity structures with the ability to change the mechanical behavior on demand.

4. EXPERIMENTAL SECTION

4.1. Materials. *N*,*N*′-Methylenebisacrylamide 97% (Bis-AAm), acrylamide (AAm), acrylic acid (AA), LAP ≥95%, citric acid ≥99.5%, and sodium citrate dihydrate ≥99% were purchased from Sigma-Aldrich. Sodium bicarbonate 99.5% was purchased from Fisher Scientific. Acryloxyethyl thiocarbamoyl rhodamine B was purchased from Polysciences, Inc. The AA monomer is passed through a short column of acidic alumina prior to use to remove the present radical inhibitor. All other chemicals are used as received without further purification.

4.2. Hydrogel Photopolymerization. The hydrogel precursors are prepared by dissolving AA and AAm monomer, Bis-AAm cross-linker (C), and LAP photoinitiator in water. Acryloxyethyl thiocarbamoyl rhodamine B is added to the hydrogel precursor solutions to enhance the visual contrast. The hydrogels are photopolymerized UV cross-linking (NailStar UV lamp 4 × 9 W bulbs, λ_{max} = 365 nm) for 60 s from precursors with varying [AA]:[AAm]:[C] concentrations.

For the classical nonentangled pAA hydrogels, the monomer concentration and monomer to cross-linker ratio [AA]:[C] are varied while fixing the photoinitiator concentration at 0.1 wt %. The hydrogel precursors for networks with high entanglement concen-

https://doi.org/10.1021/acsami.4c06610
ACS Appl. Mater. Interfaces 2024, 16, 38511−38519

trations are adapted from the reported synthesis of Nori. Here, the monomer to cross-linker ratio [AA + AAm]:[C] is kept constant at 1000:1 (= 0.1 mol % cross-linker) and the photoinitiator concentration is kept at [I]:[C] = 0.4:1.

4.3. Manufacturing of PTFE Molds. The hydrogel rods are prepared in PTFE molds: 2D computer-aided design models are milled into PTFE blocks ($X \times Y \times Z = 60 \times 30 \times 10$ mm^3) using a computer numerical control machine with a 1 mm diameter milling tool.

Swelling and actuation studies: To determine the swelling sizes at different pH, rectangular hydrogel rods ($20 \times 4 \times 2$ mm^3) or hydrogel disks (diameter = 15 mm, depth = 1.5 mm) are prepared from PTFE molds. The swelling factor $\alpha = L/L_{\text{prepared}}$ is calculated from the swollen and prepared size. The actuation strain $\varepsilon_A = 1 - L_{\text{pH2}}/L_{\text{pH9}}$ is calculated from the swollen and contracted size. The swelling difference $\beta = \alpha_{\text{active}} - \alpha_{\text{passive}}$ is calculated from the swelling factors of the active and passive hydrogels. The hidden length $L_{\text{hidden}} = L_{\text{active}} - L_{\text{passive}} = L_0 \times \beta$ is calculated from the initial length and swelling difference. The initial length, L_0 of the active strut, is 15 mm.

4.4. Sequential Photopolymerization of Hydrogels in Geometries. The passive hydrogel precursor is prepared by dissolving 5 M AAm monomer together with [AAm]:[C] = 1000:1 and [I]:[C] = 0.4:1 in water. The active hydrogel precursors are prepared by dissolving AA and AAm at [AA + AAm] = 8 M together with [AA + AAm]:[C] = 1000:1 and [I]:[C] = 0.4:1 in water. The monomer concentration of 8 M is kept constant, while the molar comonomer ratio [AA]:[AAm] is varied. We manufactured the strain-stiffening metamaterial by sequential photopolymerization: First, the active hydrogel precursor solution is filled into the mold then exposed to 15 s of UV light. Afterward, the passive hydrogel precursor solution is filled into the mold followed by UV cross-linking for 60 s. The metamaterial of depth 1.5 mm has three unit cells with a length of 9 mm, active beams of 1.5 mm width, and passive beams of 1 mm width. Figure S4 depicts all of the geometrical dimensions.

After photopolymerization, the geometry is immersed in 50 mM buffer to equilibrate overnight. Buffers for different pH values were prepared: 50 mM citric acid for pH 2; 23 mM sodium citrate dihydrate and 27 mM citric acid for pH 4.5; 43.7 mM sodium citrate dihydrate and 6.3 mM citric acid for pH 6.2; and 50 mM $NaHCO_3$ for pH 9.

4.5. Tensile Deformation Experiments. The force−displacement curves of the individual hydrogels and metamaterials equilibrated at different pH values are measured under tensile deformation with a Shimadzu compact tabletop testing machine EZ Test using a 5 N load cell and displacement rate of 1 mm s^{-1}. The hydrogels are always tensile tested after equilibration at different pH. Tensile tests on single hydrogel rods are repeated 4 times, and the standard error is calculated. The hydrogel rods and metamaterials are superglued to a paper that is clamped to reduce preliminary deformation of the hydrogel specimen.

4.6. Indentation Experiments. Because some nonentangled hydrogels could not be tensile-tested due to their high brittleness and breakage during swelling, additional indentation experiments are conducted. To this end, an Anton Paar Modular Compact Rheometer MCR 702 in compression mode with an 8 mm plate−plate geometry (PP8) is used. Four hydrogel disks (prepared in PTFE mold with 15 mm diameter and 2 mm thickness) after equilibration are measured for each composition. The hydrogels are compressed with a strain rate of 1% per second. The gap size varied between 8.8 mm and 5.2 mm depending on the equilibrated swelling size. The resulting force−displacement curves are fitted with the structural mechanics module of COMSOL Multiphysics 6.0 to extract Young's moduli. To this end, hydrogels of known stiffness values are compressed, and the resulting force−displacement curve is correlated to obtain a fitting curve.

4.7. FE Simulation. To predict the out-of-plane buckling and corresponding force−displacement curves, simulations are conducted using the structural mechanics module of COMSOL Multiphysics 6.0. The neo-Hookean material model with a hydrogel bulk Poisson's ratio of $\nu = 0.45$ and the respective Young's moduli after equilibration ($\mu_{\text{active}} = 540$ kPa, $\mu_{\text{passive}} = 54$ kPa) is employed. Half of a single unit cell is constructed and combined with a symmetry boundary condition. A rigid body suppression is applied on all domains.

Experimentally determined swelling factors α are used as an input. In the first step, the active beam swelling is predicted by thermal expansion using experimental values as input while both sides on the unit cell are constrained in the x-, y-, and z-direction. Because the active beams swell more than their surrounding frame, an insignificant gravity body force is applied in the z-axis to allow the active beams to buckle out of plane. In the second step, displacement is applied in the x-direction on one side of the unit cell while constraining the y- and z-direction. To account for the change in the cross section of the active beam after swelling, the Young's modulus is normalized accordingly. The x-component of the total reaction force required for displacement is probed.

■ ASSOCIATED CONTENT

Supporting Information

The Supporting Information is available free of charge at https://pubs.acs.org/doi/10.1021/acsami.4c06610.

Experimental details on the mechanical testing with an overview of all measured parameters, dimensions of the strain-stiffening metamaterial geometry, and swelling of active beams and metamaterials over multiple cycles with respective force−displacement curves (PDF)

Video depicting the hard and soft coding of the active beams in simulation and experiment (MP4)

■ AUTHOR INFORMATION

Corresponding Authors

Viacheslav Slesarenko − *Cluster of Excellence livMatS @ FIT—Freiburg Center for Interactive Materials and Bioinspired Technologies, University of Freiburg, 79110 Freiburg im Breisgau, Germany*; Email: viacheslav.slesarenko@livmats.uni-freiburg.de

Andreas Walther − *Life-Like Materials and Systems, Department of Chemistry, Johannes Gutenberg University Mainz, 55128 Mainz, Germany*; orcid.org/0000-0003-2170-3306; Email: andreas.walther@uni-mainz.de

Authors

Oliver Skarsetz − *Life-Like Materials and Systems, Department of Chemistry, Johannes Gutenberg University Mainz, 55128 Mainz, Germany*; orcid.org/0000-0002-1540-1873

Robin Mathes − *Life-Like Materials and Systems, Department of Chemistry, Johannes Gutenberg University Mainz, 55128 Mainz, Germany*

Ricarda Sophia Schmidt − *Life-Like Materials and Systems, Department of Chemistry, Johannes Gutenberg University Mainz, 55128 Mainz, Germany*

Moritz Simon − *Life-Like Materials and Systems, Department of Chemistry, Johannes Gutenberg University Mainz, 55128 Mainz, Germany*

Complete contact information is available at: https://pubs.acs.org/10.1021/acsami.4c06610

Notes

The authors declare no competing financial interest.

■ ACKNOWLEDGMENTS

V.S. acknowledges support by the Deutsche Forschungsgemeinschaft (DFG, German Research Foundation) under Germany's Excellence Strategy−EXC-2193/1−390951807.

A.W. acknowledges generous support from the Gutenberg Research College.

REFERENCES

(1) Storm, C.; Pastore, J. J.; MacKintosh, F. C.; Lubensky, T. C.; Janmey, P. A. Nonlinear Elasticity in Biological Gels. *Nature* **2005**, *435* (7039), 191−194.

(2) Taale, M.; Schmidt, M.; Taheri, F.; Timmermann, M.; Selhuber-Unkel, C. A Minimalistic, Synthetic Cell-Inspired Metamaterial for Enabling Reversible Strain-Stiffening. *Adv. Mater. Technol.* **2023**, *8*, 2201441.

(3) Yan, D.; Chang, J.; Zhang, H.; Liu, J.; Song, H.; Xue, Z.; Zhang, F.; Zhang, Y. Soft Three-Dimensional Network Materials with Rational Bio-Mimetic Designs. *Nat. Commun.* **2020**, *11* (1), 1180.

(4) Lin, S.; Liu, J.; Liu, X.; Zhao, X. Muscle-like Fatigue-Resistant Hydrogels by Mechanical Training. *Proc. Natl. Acad. Sci. U.S.A.* **2019**, *116* (21), 10244−10249.

(5) Hynninen, V.; Hietala, S.; McKee, J. R.; Murtomäki, L.; Rojas, O. J.; Ikkala, O.; Nonappa. Inverse Thermoreversible Mechanical Stiffening and Birefringence in a Methylcellulose/Cellulose Nanocrystal Hydrogel. *Biomacromolecules* **2018**, *19* (7), 2795−2804.

(6) De Almeida, P.; Jaspers, M.; Vaessen, S.; Tagit, O.; Portale, G.; Rowan, A. E.; Kouwer, P. H. J. Cytoskeletal Stiffening in Synthetic Hydrogels. *Nat. Commun.* **2019**, *10* (1), 609.

(7) Kouwer, P. H. J.; Koepf, M.; Le Sage, V. A. A.; Jaspers, M.; Van Buul, A. M.; Eksteen-Akeroyd, Z. H.; Woltinge, T.; Schwartz, E.; Kitto, H. J.; Hoogenboom, R.; Picken, S. J.; Nolte, R. J. M.; Mendes, E.; Rowan, A. E. Responsive Biomimetic Networks from Polyisocyanopeptide Hydrogels. *Nature* **2013**, *493* (7434), 651−655.

(8) Liu, Y.; Lin, S.-H.; Chuang, W.-T.; Dai, N.-T.; Hsu, S. Biomimetic Strain-Stiffening in Chitosan Self-Healing Hydrogels. *ACS Appl. Mater. Interfaces* **2022**, *14* (14), 16032−16046.

(9) Bertula, K.; Martikainen, L.; Munne, P.; Hietala, S.; Klefström, J.; Ikkala, O.; Nonappa. Strain-Stiffening of Agarose Gels. *ACS Macro Lett.* **2019**, *8* (6), 670−675.

(10) Berger, J. B.; Wadley, H. N. G.; McMeeking, R. M. Mechanical Metamaterials at the Theoretical Limit of Isotropic Elastic Stiffness. *Nature* **2017**, *543* (7646), 533−537.

(11) Bertoldi, K.; Vitelli, V.; Christensen, J.; Van Hecke, M. Flexible Mechanical Metamaterials. *Nat. Rev. Mater.* **2017**, *2* (11), 17066.

(12) Kolken, H. A.; Zadpoor, A. A. Auxetic Mechanical Metamaterials. *RSC Adv.* **2017**, *7* (9), 5111−5129.

(13) Babaee, S.; Shim, J.; Weaver, J. C.; Chen, E. R.; Patel, N.; Bertoldi, K. 3D Soft Metamaterials with Negative Poisson's Ratio. *Adv. Mater.* **2013**, *25* (36), 5044−5049.

(14) Bückmann, T.; Stenger, N.; Kadic, M.; Kaschke, J.; Frölich, A.; Kennerknecht, T.; Eberl, C.; Thiel, M.; Wegener, M. Tailored 3D Mechanical Metamaterials Made by Dip-in Direct-Laser-Writing Optical Lithography. *Adv. Mater.* **2012**, *24* (20), 2710−2714.

(15) Mirzaali, M. J.; Janbaz, S.; Strano, M.; Vergani, L.; Zadpoor, A. A. Shape-Matching Soft Mechanical Metamaterials. *Sci. Rep.* **2018**, *8* (1), 965.

(16) Wenz, F.; Schmidt, I.; Leichner, A.; Lichti, T.; Baumann, S.; Andrae, H.; Eberl, C. Designing Shape Morphing Behavior through Local Programming of Mechanical Metamaterials. *Adv. Mater.* **2021**, *33* (37), 2008617.

(17) Schwarz, D.; Felsch, G.; Tauber, F.; Schiller, S.; Slesarenko, V. Exploiting Self-Contact in Mechanical Metamaterials for New Discrete Functionalities. *Mater. Des.* **2023**, *236*, 112468.

(18) Liang, X.; Crosby, A. J. Uniaxial Stretching Mechanics of Cellular Flexible Metamaterials. *Extreme Mech. Lett.* **2020**, *35*, 100637.

(19) Kotikian, A.; Watkins, A. A.; Bordiga, G.; Spielberg, A.; Davidson, Z. S.; Bertoldi, K.; Lewis, J. A. Liquid Crystal Elastomer Lattices with Thermally Programmable Deformation via Multi-Material 3D Printing. *Adv. Mater.* **2024**, 2310743.

(20) Wang, Z.; Wang, Z.; Zheng, Y.; He, Q.; Wang, Y.; Cai, S. Three-Dimensional Printing of Functionally Graded Liquid Crystal Elastomer. *Sci. Adv.* **2020**, *6* (39), No. eabc0034.

(21) Li, S.; Librandi, G.; Yao, Y.; Richard, A. J.; Schneider-Yamamura, A.; Aizenberg, J.; Bertoldi, K. Controlling Liquid Crystal Orientations for Programmable Anisotropic Transformations in Cellular Microstructures. *Adv. Mater.* **2021**, *33* (42), 2105024.

(22) Li, S.; Deng, B.; Grinthal, A.; Schneider-Yamamura, A.; Kang, J.; Martens, R. S.; Zhang, C. T.; Li, J.; Yu, S.; Bertoldi, K.; Aizenberg, J. Liquid-Induced Topological Transformations of Cellular Microstructures. *Nature* **2021**, *592* (7854), 386−391.

(23) Yang, C.; Boorugu, M.; Dopp, A.; Ren, J.; Martin, R.; Han, D.; Choi, W.; Lee, H. 4D Printing Reconfigurable, Deployable and Mechanically Tunable Metamaterials. *Mater. Horiz.* **2019**, *6* (6), 1244−1250.

(24) van Manen, T.; Janbaz, S.; Jansen, K. M. B.; Zadpoor, A. A. 4D Printing of Reconfigurable Metamaterials and Devices. *Commun. Mater.* **2021**, *2* (1), 56.

(25) Jackson, J. A.; Messner, M. C.; Dudukovic, N. A.; Smith, W. L.; Bekker, L.; Moran, B.; Golobic, A. M.; Pascall, A. J.; Duoss, E. B.; Loh, K. J.; Spadaccini, C. M. Field Responsive Mechanical Metamaterials. *Sci. Adv.* **2018**, *4* (12), No. eaau6419.

(26) Montgomery, S. M.; Wu, S.; Kuang, X.; Armstrong, C. D.; Zemelka, C.; Ze, Q.; Zhang, R.; Zhao, R.; Qi, H. J. Magneto-Mechanical Metamaterials with Widely Tunable Mechanical Properties and Acoustic Bandgaps. *Adv. Funct. Mater.* **2021**, *31* (3), 2005319.

(27) Zou, B.; Liang, Z.; Zhong, D.; Cui, Z.; Xiao, K.; Shao, S.; Ju, J. Magneto-thermomechanically Reprogrammable Mechanical Metamaterials. *Adv. Mater.* **2023**, *35*, 2207349.

(28) Sim, J.; Wu, S.; Dai, J.; Zhao, R. R. Magneto-Mechanical Bilayer Metamaterial with Global Area-Preserving Density Tunability for Acoustic Wave Regulation. *Adv. Mater.* **2023**, *35* (35), 2303541.

(29) Skarsetz, O.; Slesarenko, V.; Walther, A. Programmable Auxeticity in Hydrogel Metamaterials via Shape-Morphing Unit Cells. *Adv. Sci.* **2022**, *9* (23), 2201867.

(30) Zhang, M.; Pal, A.; Zheng, Z.; Gardi, G.; Yildiz, E.; Sitti, M. Hydrogel Muscles Powering Reconfigurable Micro-Metastructures with Wide-Spectrum Programmability. *Nat. Mater.* **2023**, *22* (10), 1243−1252.

(31) Dong, M.; Han, Y.; Hao, X. P.; Yu, H. C.; Yin, J.; Du, M.; Zheng, Q.; Wu, Z. L. Digital Light Processing 3D Printing of Tough Supramolecular Hydrogels with Sophisticated Architectures as Impact-Absorption Elements. *Adv. Mater.* **2022**, *34* (34), 2204333.

(32) Bai, Y.; Liu, C.; Li, Y.; Li, J.; Qiao, L.; Zhou, J.; Bai, Y. Moisture-Sensitive Mechanical Metamaterials with Unusual and Re-Programmable Hygroscopic Deformation Modes. *Mater. Horiz.* **2022**, *9* (11), 2835−2845.

(33) Zhang, H.; Guo, X.; Wu, J.; Fang, D.; Zhang, Y. Soft Mechanical Metamaterials with Unusual Swelling Behavior and Tunable Stress-Strain Curves. *Sci. Adv.* **2018**, *4* (6), No. eaar8535.

(34) Gong, J. P.; Katsuyama, Y.; Kurokawa, T.; Osada, Y. Double-Network Hydrogels with Extremely High Mechanical Strength. *Adv. Mater.* **2003**, *15* (14), 1155−1158.

(35) Lin, S.; Londono, C. D.; Zheng, D.; Zhao, X. An Extreme Toughening Mechanism for Soft Materials. *Soft Matter* **2022**, *18* (31), 5742−5749.

(36) Sun, J. Y.; Zhao, X.; Illeperuma, W. R. K.; Chaudhuri, O.; Oh, K. H.; Mooney, D. J.; Vlassak, J. J.; Suo, Z. Highly Stretchable and Tough Hydrogels. *Nature* **2012**, *489* (7414), 133−136.

(37) Rikkou-Kalourkoti, M.; Kitiri, E. N.; Patrickios, C. S.; Leontidis, E.; Constantinou, M.; Constantinides, G.; Zhang, X.; Papadakis, C. M. Double Networks Based on Amphiphilic Cross-Linked Star Block Copolymer First Conetworks and Randomly Cross-Linked Hydrophilic Second Networks. *Macromolecules* **2016**, *49* (5), 1731−1742.

(38) Norioka, C.; Inamoto, Y.; Hajime, C.; Kawamura, A.; Miyata, T. A Universal Method to Easily Design Tough and Stretchable Hydrogels. *NPG Asia Mater.* **2021**, *13* (1), 34.

(39) Kim, J.; Zhang, G.; Shi, M.; Suo, Z. Fracture, Fatigue, and Friction of Polymers in Which Entanglements Greatly Outnumber Cross-Links. *Science* **2021**, *374* (6564), 212−216.

(40) Xiao, S.; Zhang, M.; He, X.; Huang, L.; Zhang, Y.; Ren, B.; Zhong, M.; Chang, Y.; Yang, J.; Zheng, J. Dual Salt- and

https://doi.org/10.1021/acsami.4c06610
ACS Appl. Mater. Interfaces 2024, 16, 38511−38519

Thermoresponsive Programmable Bilayer Hydrogel Actuators with Pseudo-Interpenetrating Double-Network Structures. *ACS Appl. Mater. Interfaces* **2018**, *10* (25), 21642−21653.
(41) Chen, Y.; Wu, W.; Yu, J.; Wang, Y.; Zhu, J.; Hu, Z. Mechanical Strong Stretchable Conductive Multi-Stimuli-Responsive Nanocomposite Double Network Hydrogel as Biosensor and Actuator. *J. Biomater. Sci., Polym. Ed.* **2020**, *31* (14), 1770−1792.
(42) Zhang, J.; Zeng, L.; Qiao, Z.; Wang, J.; Jiang, X.; Zhang, Y. S.; Yang, H. Functionalizing Double-Network Hydrogels for Applications in Remote Actuation and in Low-Temperature Strain Sensing. *ACS Appl. Mater. Interfaces* **2020**, *12* (27), 30247−30258.

https://doi.org/10.1021/acsami.4c06610
ACS Appl. Mater. Interfaces 2024, 16, 38511−38519